Supporting Information

Recyclable Fe_3O_4/MWCNT/CNF Composite Nanopaper as an Advanced Negative Electrode for Flexibility Asymmetric Supercapacitors

Haoran Zhao [a], Haidong Jin[a], Shenghui Li[a], Yahui Dong [a], Shipeng Wang [a], Qian Cheng[a,*], Yu Li [b,*]

[a] *Key Laboratory of Bio-based Material Science & Technology(Ministry of Education), College of Material Science and Engineering, Northeast Forestry University, Harbin 150040, China*

[b] *College of Science, Northeast Forestry University, Harbin 150040,China*

*Corresponding author. *E-mail addresses*: chengqian66@163.com(Q. Cheng)
liyu87043@163.com (Y. Li)

Figure Content

Calculation methods

Fig. S9(a-f). The GCD curves of (a) NFT@Fe-802, (b) NFT@Fe-622,(c) NFT@Fe-532 and (d) NFT@Fe-442 at different current densities; (e) the variation in the specific capacitance of the NFT@Fe-xyz nanopaper samples at different current densities; (f) long-term cycling performance of the NFT@Fe-712 at a current density of 5 A g^{-1} (inset shows the GCD curves of the last 10 cycles).

Fig. S10. (a) SEM images, (b) elemental mapping of C, O, Fe, S, and (c) XRD of NFT@Fe-712 after long-term cycling

Table S3. Equivalent series resistance of the NFT@Fe-xyz nanopaper samples

References

Calculation methods

Specific capacitance (C_p, F g^{-1}) with respect to a single electrode was calculated using CV profiles at different scan rates.

$$C_P = \frac{\int Idv}{2v\, m\, \Delta V} \#(S1)$$

Where, $\int I$dv is the area under CV curve, v is the potential scan rate (V s^{-1}), m (g) is the mass of electrode and ΔV (V) is the potential window.

The mass capacitance of single electrode was estimated from the GCD curves at different current density using equations:

$$C_p = \frac{I\, \Delta t}{m\, \Delta V} \#(S2)$$

Where I (A) is the discharge current, Δt (s) is the discharge time for potential window ΔV (V) and m (g) is the mass of electrode. To calculate areal capacitance, m (g) has been replaced with electrode area A (cm^{-2}).

To identify the combined characteristics of electrochemical capacitive and diffusion controlled processes of NFT@Fe, the relationship of current density (i) and corresponding the scan rate (v) can be evaluated the following equation:

$$i = av^b \#(S3)$$

$$\log{(i)} = blog(v) + \log{(a)} \#(S4)$$

Where, a and b present constants. The linear relationship between log (i) and log (v) can provide the value of b, which is an important indicator for evaluating the kinetics of redox reaction.

The dependence of voltametric current on scan rate form CV was used to calculate the capacitance proportion.

$$i(V) = K_1 v + K_2 v^{1/2} \#(S5)$$

$$\frac{i(V)}{v^{1/2}} = K_1 v^{1/2} + K_2 \#(S6)$$

Where, *i* represents a current density at the potential of *V*, $K_1 v$ and $K_2 v^{1/2}$ are the current contribute in capacitive-controlled and diffusion-controlled processes.

For a flexible asymmetric supercapacitor, charge balance between positive and negative electrodes follows equations:

$$Q^+ = Q^- \#(S7)$$

$$Q^+ = C_p{}^+ \Delta V m^+ \#(S8)$$

$$Q^- = C_p{}^- \Delta V m^- \#(S9)$$

In which Q^+ and Q^- are the charge stored in positive and negative electrode, ΔV is the voltage window during the charge and discharge process. m^+ and m^- are the mass of positive and negative electrode, respectively.

C_p (F g^{-1}), energy density (E, Wh kg^{-1}) and power density (P, W kg^{-1}) of ASC were evaluated using following equations:

$$E = \frac{0.5\, C_p\, \Delta V^2}{3.6} \#(S10)$$

$$P = \frac{3600\, E}{\Delta t} \#(S11)$$

Table S1. The raw materials ratio of the NFT@Fe-xyz nanopapers

Sample	MWCNT@Fe_3O_4 /mg	MWCNT /mg	CNF /mg	Mass ratio
NFT@Fe-505	20	0	20	5:0:5
NFT@Fe-604	24	0	16	6:0:4
NFT@Fe-703	28	0	12	7:0:3
NFT@ Fe-802	32	0	8	8:0:2
NFT@ Fe-901	36	0	4	9:0:1
NFT@ Fe-712	28	4	8	7:1:2
NFT@ Fe-622	24	8	8	6:2:2
NFT@ Fe-532	20	12	8	5:3:2
NFT@ Fe-442	16	16	8	4:4:2
NFT	0	32	8	0:8:2

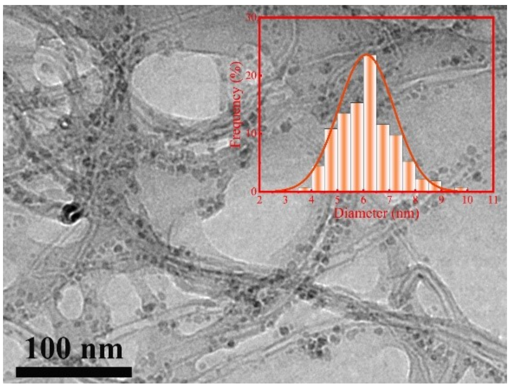

Fig. S1. TEM images of MWCNT@Fe_3O_4 (the inset shows the size distribution of Fe_3O_4 nanoparticles)

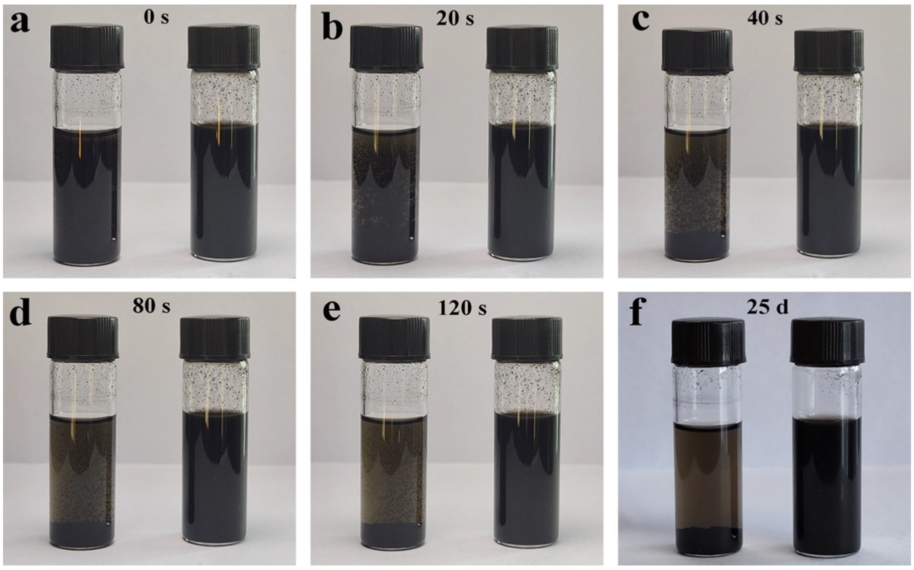

Fig. S2. Digital photographs of the MWCNT@Fe_3O_4 composites dispersed in ethanol (left) and CNF (right) standing for (a) 0 s, (b) 20 s, (c) 40 s, (d) 80 s, (e) 120 s, and (f) 25 d

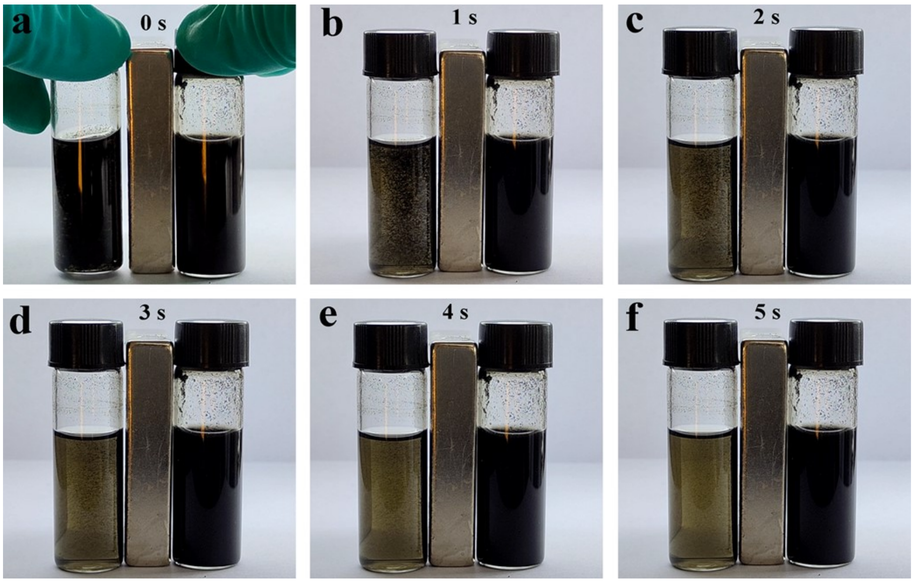

Fig. S3. Digital photographs of MWCNT@Fe_3O_4 composites dispersed in ethanol (left) and CNF (right) at sides of the magnet after (a) 0, (b) 1, (c) 2, (d) 3, (e) 4, and (f) 5 s.

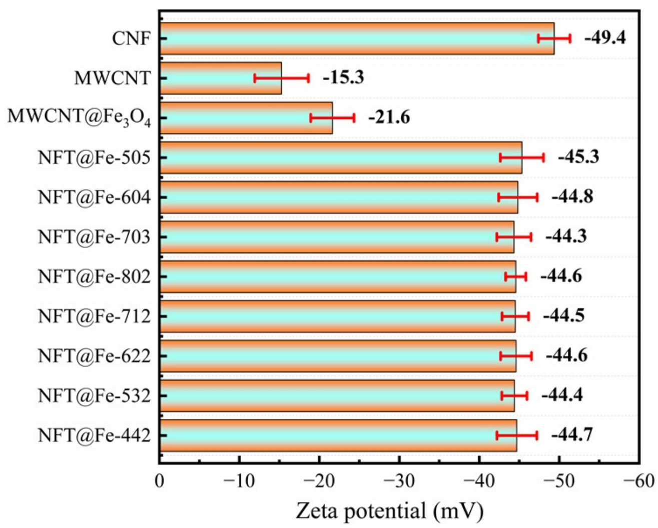

Fig. S4. The zeta potential of CNF, MWCNT, MWCNT@Fe_3O_4, and NFT@Fe-xyz.

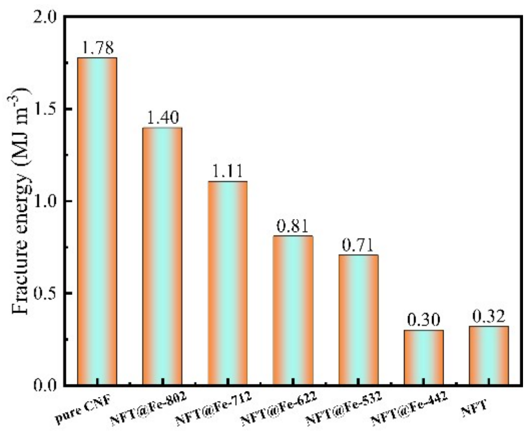

Fig. S5. The fracture energy of the NFT and NFT@Fe-xyz.

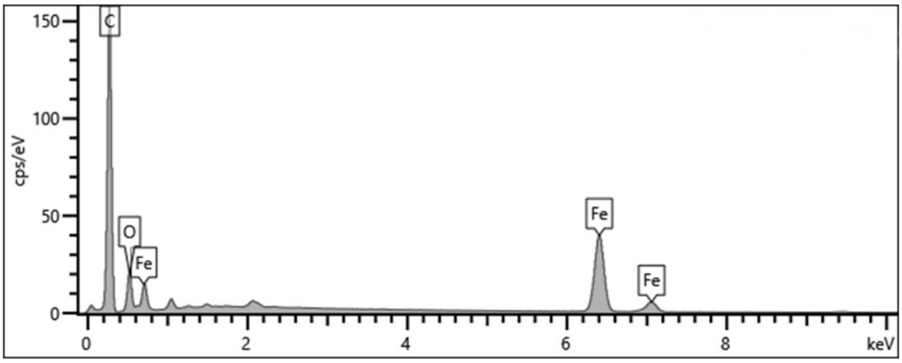

Fig. S6. The EDS spectrum of the NFT@Fe-712 composite nanopaper.

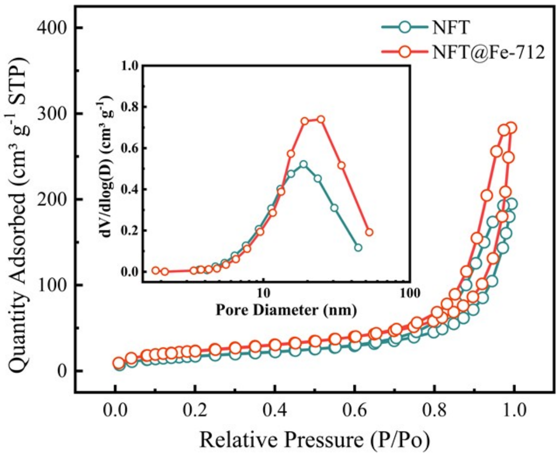

Fig. S7. N_2 adsorption–desorption isotherms and corresponding BJH pore-size distribution curves (inset) of the NFT@Fe-712 and NFT

Table S2. Comparison of the reported Fe_3O_4-based electrode and flexible cellulose-based electrodes

Materials	Specific capacitance	Scan rate ($mV\ s^{-1}$)	Current density	Reference
Fe_3O_4-rGO	270 $F\ g^{-1}$	5	-	1
Fe_3O_4@Fe_2O_3	231.9 $F\ g^{-1}$	5	-	2
NCS@Fe_3O_4	206 $F\ g^{-1}$	-	1 $A\ g^{-1}$	3
Fe_3O_4/Carbon Nanofiber	135 $F\ g^{-1}$	5	-	4
Fe_3O_4-C	102 $F\ g^{-1}$	5	-	5
CNF/MWCNT/RGO/Fe_3O_4	169.3 $F\ g^{-1}$	-	1 $mA\ cm^{-2}$	6
CNF/porous Co_3O_4	594.8 $mF\ cm^{-2}$	5	-	7
PH-MWCNT(90-10 wt%)	121 $mF\ cm^{-2}$	5	-	8
CNF/MWCNT aerogel	114.8 $F\ g^{-1}$	10	-	9
CNF/CNT/RGO-3	116.3 $F\ g^{-1}$	-	0.1 $A\ g^{-1}$	10
FWCNT/CNF buckypaper	167.6 $F\ g^{-1}$	5	-	11
RGO/CNC	176.7 $F\ g^{-1}$ (4.42 $mF\ cm^{-2}$)	-	0.5 $A\ g^{-1}$	12
NFT@Fe-712	229.9 $F\ g^{-1}$ (735.68 $mF\ cm^{-2}$)	5	-	This work
NFT@Fe-712	210.8 $F\ g^{-1}$ (674.56 $mF\ cm^{-2}$)	-	0.5 $A\ g^{-1}$	This work

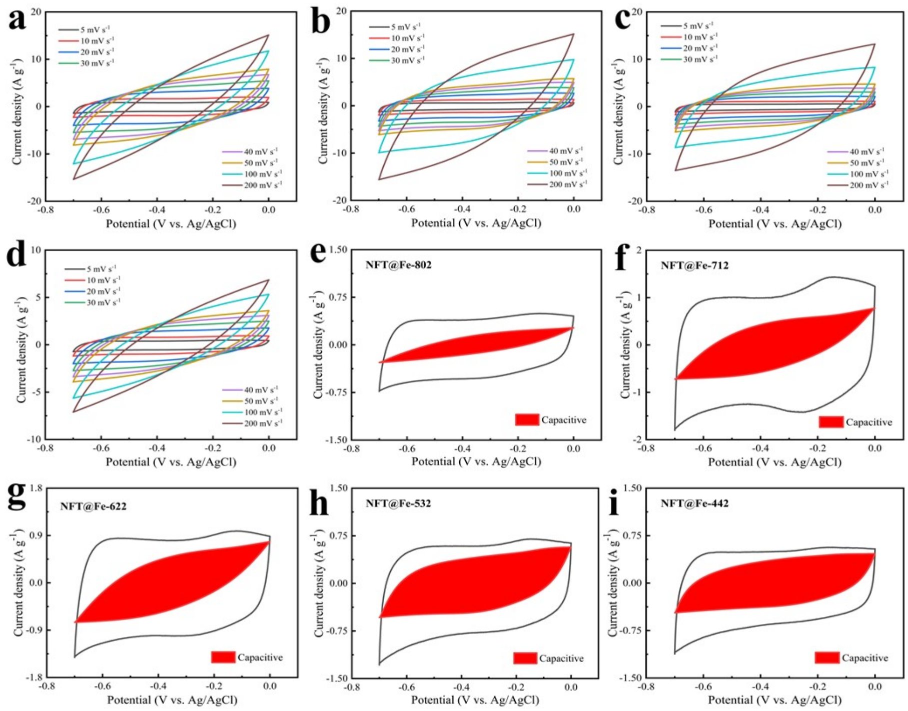

Fig. S8. The CV curves of (a) NFT@Fe-622, (b) NFT@Fe-532, (c) NFT@Fe-442, and (d) NFT@Fe-802 at different scan rates and the capacitive contributions at 5 mV s^{-1} of (e) NFT@Fe-802, (f) NFT@Fe-712, (g) NFT@Fe-622, (h) NFT@Fe-532, and (i) NFT@Fe-442.

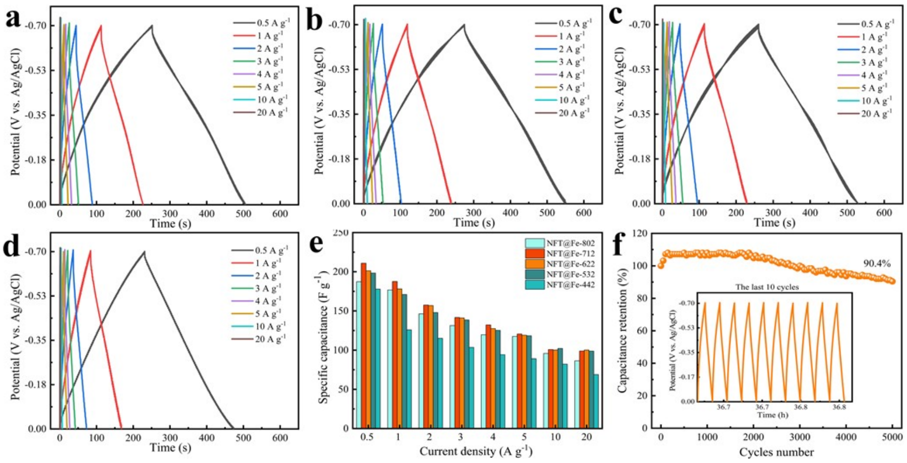

Fig. S9. The GCD curves of (a) NFT@Fe-802, (b) NFT@Fe-622,(c) NFT@Fe-532 and (d) NFT@Fe-442 at different current densities; (e) the variation in the specific capacitance of the NFT@Fe-xyz nanopaper samples at different current densities; (f) long-term cycling performance of the NFT@Fe-712 at a current density of 5 A g^{-1} (inset shows the GCD curves of the last 10 cycles).

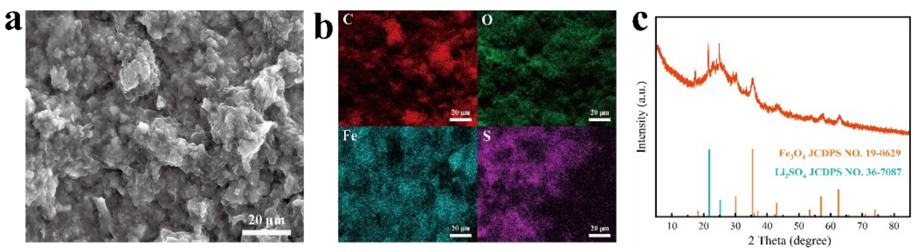

Fig. S10. (a) SEM images, (b) elemental mapping of C, O, Fe, S, and (c) XRD of NFT@Fe-712 after long-term cycling

Table S3. Equivalent series resistance of the NFT@Fe-xyz nanopaper samples

Sample	Solution resistance (R_s /Ω)	Charge transfer resistance (R_{ct} /Ω)	Warburg impedance (R_w /Ω)	Equivalent series Resistance (R_{es} /Ω)
NFT@Fe-802	2.875	7.105	7.143	17.123
NFT@Fe-712	1.828	3.862	4.133	9.823
NFT@Fe-622	1.558	3.068	2.019	6.645
NFT@Fe-532	1.703	1.775	2.380	5.858
NFT@Fe-442	1.486	1.407	1.391	4.284

Reference

1. T. Qi, J. Jiang, H. Chen, H. Wan, L. Miao and L. Zhang, *Electrochim. Acta*, 2013, **114**, 674-680.
2. X. Tang, R. Jia, T. Zhai and H. Xia, *ACS Appl. Mater. Interfaces*, 2015, **7**, 27518-27525.
3. X. Zhu, D. Hou, H. Tao and M. Li, *J. Alloys Compd.*, 2020, **821**, 153580.
4. J. Mu, B. Chen, Z. Guo, M. Zhang, Z. Zhang, P. Zhang, C. Shao and Y. Liu, *Nanoscale*, 2011, **3**, 5034-5040.
5. L. Li, P. Gao, S. Gai, F. He, Y. Chen, M. Zhang and P. Yang, *Electrochim. Acta*, 2016, **190**, 566-573.
6. L. Xia, X. Li, X. Wu, L. Huang, Y. Liao, Y. Qing, Y. Wu and X. Lu, *J. Mater. Chem. A*, 2018, **6**, 17378-17388.

7. L. Xiao, H. Qi, K. Qu, C. Shi, Y. Cheng, Z. Sun, B. Yuan, Z. Huang, D. Pan and Z. Guo, *Adv. Compos. Hybrid Mater.*, 2021, **4**, 306-316.
8. V.-P. Vu, V.-D. Mai, D. C. T. Nguyen and S.-H. Lee, *ACS Appl. Energy Mater.*, 2022, **5**, 2211-2220.
9. D.-C. Wang, H.-Y. Yu, Z. Ouyang, D. Qi, Y. Zhou, A. Ju, Z. Li and Y. Cao, *Nanoscale*, 2022, **14**, 5163-5173.
10. H. y. Liu, T. Xu, C. y. Cai, K. Liu, W. Liu, M. Zhang, H. s. Du, C. l. Si and K. Zhang, *Adv. Funct. Mater.*, 2022, **32**, 2113082.
11. F. A. Denis, J. Mario Guimarães, C. G. S. Mayara, S. P. Paula, H. R. d. C. Thiago, C. D. Matheus, L. L. Rodrigo and F. R. O. Paulo, *J. Energy Storage*, 2022, **52**, 104848.
12. Z. Ding, Y. Tang and P. Zhu, *Int. J. Biol. Macromol.*, 2022, **200**, 574-582.